A Surface Flow Approach for Predicting Crosshatch Patterns

R. M. GRABOW* AND C. O. WHITE†
Aeronutronic Division of Philco-Ford Corporation, Newport Beach, Calif.

An analytical model based on liquid layer stability theory is used to predict the stability characteristics and geometric features of crosshatched ablation patterns. This approach postulates the formation of a melt or viscoelastic layer which interacts with the gas boundary layer. For supersonic flow, the dominant amplifying effect is found to be the component of the gas pressure perturbation acting in the valleys of the surface waves, while the dominant damping effect is the component of the gas shear perturbation acting on the wave slope. Solutions for the rate of amplification yield parameters that characterize pattern onset, wave angle, wavelength, and depth. Correlations with experimental data show reasonably good agreement.

Nomenclature

c = complex wave velocity
c_p = pressure coefficient
g = body force normal to surface
h = pattern depth
K_m = material constant
M = Mach number
$\tilde{M}$ = molecular weight
p = pressure
$\hat{P}_{\text{mag}}$ = amplitude of pressure perturbation
Re = Reynolds number of surface flow layer
t = time
T = temperature
u_L = velocity at edge of surface flow layer
x, y, z = Cartesian coordinates of surface (Fig. 2)
x_N = coordinate normal to wave crests
α = dimensionless wave number
β = Mach angle
γ = ratio of specific heats
Γ = body force parameter
δ = boundary layer thickness
δ_f = viscous sublayer thickness
δ_L = surface flow thickness
ε = amplitude of surface wave
λ_L, λ_z = wavelengths in streamwise and lateral directions
λ_N = wavelength normal to wave crests
μ_L = viscosity of surface flow layer
Π = complex pressure perturbation parameter
ρ_L = density of surface flow layer
σ = surface tension
Σ = complex shear perturbation parameter
τ = shear stress
T = surface tension parameter
ϕ_p = pressure phase angle
ω = wave angle
Ω_p = sublayer perturbation parameter

Subscripts
e = edge of boundary layer value
i = imaginary part of complex variable
mag = amplitude of perturbed quantity
N = normal to waves
o = neutral stability condition
r = real part of complex variable
w = wavy surface condition

Superscripts
$(\,)'$ = perturbation value
$(\bar{\ })$ = dimensional quantity

Presented as Paper 72-718 at the AIAA 5th Fluid and Plasma Dynamics Conference, Boston, Mass., June 26–28, 1972; submitted August 3, 1972; revision received November 8, 1972. This work was supported by Air Force Space and Missile Systems Organization, Contract F04701-71-C-0014.

Index categories: Supersonic and Hypersonic Flow; Material Ablation.

* Section Supervisor, Aerothermodynamics. Member AIAA.
† Staff Member, Systems Engineering. Member AIAA.

I. Introduction

THE subject of crosshatched surface patterns has been pursued both theoretically and experimentally by numerous investigators. A comprehensive summary of the existing data and theories has recently been reported.[1,2] The theoretical work included the mechanisms of: Differential Ablation,[3-5] Inelastic Deformation,[6,7] and Liquid Layer Instability.[8] An example of experimental data that was used to evaluate the various theories is shown in Fig. 1. This Teflon cone was exposed to a rocket motor exhaust flow having a large favorable pressure gradient in the axial direction. As a result, the afterbody remained smooth, the midsection had orderly crosshatching, while the forward section had severe scalloping. Given the distribution of flowfield parameters along the body, each theory was examined to determine if it could quantitatively or even qualitatively predict the observed phenomena. The inelastic deformation and liquid layer mechanisms appeared to explain the trends displayed by Teflon as well as numerous other materials. However, none of the theories was able to provide quantitative results that were in agreement with the data. Subsequently, the present authors developed a new approach which included both mechanisms and was capable of correlating most of the experimental data. This paper describes the approach, the data correlations, and the resulting prediction technique.

II. Analytical Approach

General Description

The approach developed in this paper is based on a surface flow mechanism which requires the existence of a melt layer

Fig. 1 Crosshatch patterns on teflon cone; rocket motor test condition.

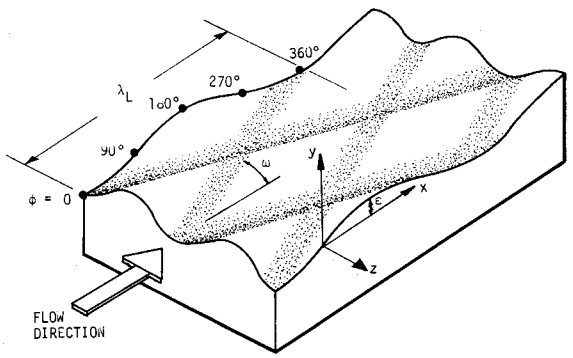

Fig. 2 Geometry of crosshatched surface.

or viscoelastic (inelastically deformable) layer. This layer becomes dynamically disturbed upon interaction with the external boundary-layer flow, and several competing factors tend to amplify or dampen the disturbance motion. If the amplifying factors are dominant, surface waves occur, which result in the type of three-dimensional crosshatched geometry shown in Fig. 2. A stability analysis is required to predict the conditions under which these waves occur, and the resulting pattern characteristics (wavelength λ_L, wave angle ω, and amplitude ε).

The analysis employs a three-layer model to characterize the interaction of the surface with the boundary-layer flow. As depicted in Fig. 3, the surface flow (melt or viscoelastic) layer has an unstable interface with the adjacent gas sublayer, and the disturbance motion is propagated through the sublayer to the external flow. The velocity profiles are assumed to be linear in the surface and sublayer flows, while the external flow velocity profile is characteristic of a fully turbulent flow. For simplicity, viscosity is neglected in the treatment of the external flow, but is included in the sublayer flow analysis. It is interesting to note that this three-layer model was independently proposed by Hains,[9] as being necessary to prove the similarity between supersonic ablation patterns and beach erosion patterns. The concept of a viscous sublayer between a responsive surface and a supersonic external flow is analogous to a thin liquid layer between an eroding beach and a hydrodynamically supercritical external flow. The following paragraphs describe the methods used to analyze each component of the three-layer model.

Surface Flow Analysis

The first application of a surface flow mechanism to the cross-hatching problem is credited to Nachtsheim.[8] His analysis considered the interaction of a liquid layer with a uniform supersonic gas flow. The present approach differs from Nachtsheim's work by permitting a surface flow layer to interact with a nonuniform viscous sublayer contained within a nonuniform inviscid flow.

The present treatment of the surface flow layer is based on the liquid layer stability analysis of Craik.[10] As demonstrated by Lane,[7] liquid layer methodology is applicable to viscoelastic layers when the liquid viscosity is replaced by an effective viscosity that is frequency dependent in accordance with the inelastic deformation model. For this investigation, it is assumed that such a viscosity is available from experimental data and can be used directly in the liquid layer analysis. Since Craik's analysis is two-dimensional, it must be applied normal to the oblique waves. The disturbed surface in the normal direction x_N is represented by a sinusoidal waviness of amplitude

$$\varepsilon = \varepsilon_0 \exp\{i\bar{\alpha}(x_N - \bar{c}t)\} \quad \text{where} \quad \bar{\alpha} = 2\pi/\lambda_N \tag{1}$$

The stability analysis of the surface flow layer involves solutions to the Orr-Sommerfeld equation by small perturbation techniques. For the case of long wavelengths and small surface flow Reynolds numbers (which is appropriate for supersonic cross-hatching problems), Craik's closed-form amplification rate solution is

$$\alpha c_i = \tfrac{1}{3}\alpha^2 Re[\Pi_r + (3\Sigma_i/2\alpha) - T\alpha^2 - \Gamma] \tag{2}$$

where

$\alpha = \bar{\alpha}\delta_L = 2\pi\delta_L/\lambda_N$ wave number normal to waves

$c = \bar{c}/u_L$ complex wave velocity

$Re = \rho_L u_L \delta_L/\mu_L$ Reynolds number of surface flow

$T = \sigma/(\rho_L {u_L}^2 \delta_L)$ surface tension parameter

$\Gamma = g\delta_L/{u_L}^2$ body force parameter

$\Pi = p_w'\delta_L/(\rho_L {u_L}^2 \varepsilon)$ complex pressure perturbation parameter

$\Sigma = \tau_w'\delta_L/(\rho_L {u_L}^2 \varepsilon)$ complex shear perturbation parameter

This solution has also been derived by Nayfeh and Saric,[11] who generalized the body force effect to include arbitrary direction. It is noted that the real parts of complex variables are in phase with the wave displacement, while the imaginary parts are in phase with the wave slope.

Viscous Sublayer Flow Analysis

The treatment of the two-dimensional viscous sublayer flow in a direction normal to the waves is based on the work of Inger,[4] who defined this region as one which contains all the viscosity and heat conduction effects on the disturbed flowfield. In the case of a turbulent boundary layer, this viscous disturbance sublayer lies within the conventional "laminar sublayer," and has a thickness

$$\delta_f = [{\mu_w}^2/(\rho_w \tau_{w_N} \bar{\alpha})]^{1/3} \tag{3}$$

In terms of the present complex variable notation,‡ Inger's closed-form solution for the sublayer shear-stress perturbation in the low heat transfer case is

$$\tau_{w_N}' = 1.37\tau_{w_N} \frac{\varepsilon\Omega p}{\delta_f} e^{(2\pi/3)i} \tag{4}$$

which reveals a phase degree of 120° relative to the pressure perturbation. The quantity

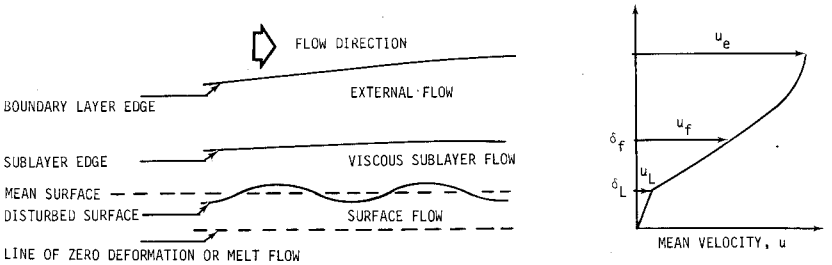

Fig. 3 Schematic of surface flow model.

‡ The complex variable notation of Craik is used rather than the notation previously employed by the authors in Refs. 2 and 13, which resulted in phasing errors.

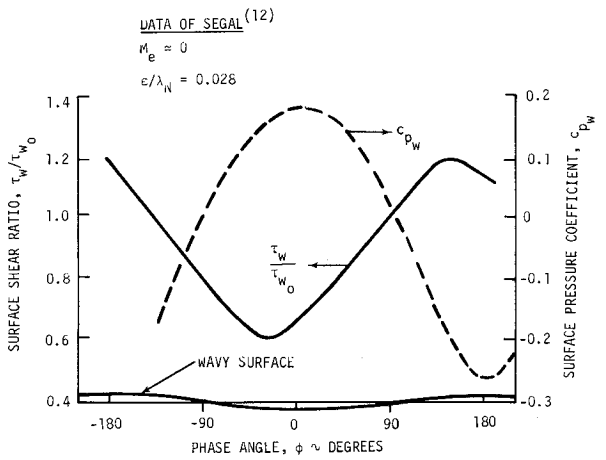

Fig. 4 Wavy surface shear and pressure phasing.

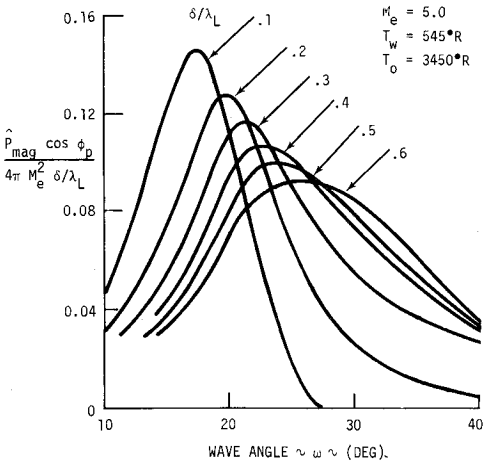

Fig. 5 Pressure perturbation in surface valley; Donaldson-Conrad theory.

$$\Omega_p = \bar{\alpha}\delta_f{}^2 p_w'/(\varepsilon\tau_{w_N})$$

is the ratio of pressure to viscous forces in the sublayer perturbation field. We now represent the pressure perturbation by an amplitude $(p_w')_{mag}$ and a phase angle (ϕ_p) measured from the valley of the wavy surface (Fig. 2). The shear perturbation can then be written in the form

$$\tau_{w_N}' = 1.37\gamma\alpha^{2/3} p_e \left(\frac{\varepsilon}{\delta}\right)\left(\frac{u_w{}^2}{\rho_w \tau_{w_N}}\right)^{1/3} \hat{P}_{mag}\, e^{(\phi_p + 2\pi/3)i} \tag{5}$$

where

$$\hat{P}_{mag} = \frac{(p_w'/p_e)_{mag}}{\gamma(\varepsilon/\delta)} \tag{6}$$

is the dimensionless pressure perturbation amplitude in the notation used by Kubota.[5] For use in the surface flow amplification rate solution [Eq. (2)], the imaginary part of the complex shear perturbation parameter is

$$\Sigma_i = 1.37\gamma\alpha^{2/3} \frac{p_e}{\rho_L u_L{}^2}\left(\frac{\delta_L}{\delta}\right)\left(\frac{\mu_w{}^2}{\rho_w \tau_{w_N}}\right)^{1/3} \hat{P}_{mag} \sin(\phi_p + 120) \tag{7}$$

The phase lag of 120° between the pressure and shear perturbations agrees with Craik's incompressible flow solution.[10] At low speeds, the wavy wall skin friction and pressure data of Segal[12] shown in Fig. 4 reveals that the maximum shear occurs at a phase angle of 140°, while the maximum pressure occurs in the valleys ($\phi_p = 0$). For the same value of δ/λ_N at supersonic speeds, the maximum pressure would theoretically occur at a larger phase angle,[3-5] and in this case, a 140° phase lag would place the maximum shear closer to the crests of the waves. This is an important result which needs to be confirmed by experimental data.

External Flow Analysis

The treatment of the external flow is based on inviscid solutions for the nonuniform flow over a wavy surface. For the case of two-dimensional flow over a surface described by $\varepsilon = \varepsilon_0 \exp(2\pi x_N/\lambda_N)i$, the results of Kubota[5] or Inger[4] may be employed. Both these investigators solved the inviscid Lighthill equation for a continuous turbulent boundary-layer Mach number profile.

For the case of a three-dimensional, crosshatched surface waviness described by the general Fourier component

$$\varepsilon = \varepsilon_0 \exp(2\pi x/\lambda_L + 2\pi z/\lambda_z)i \tag{8}$$

the present analysis employs the results of Donaldson and Conrad.[3] Their method consists of segmenting the nonuniform external flow into a large number of uniform flow strips. The pressure perturbation in each strip is evaluated by linearized inviscid theory and the perturbations and streamline directions are matched at the interfaces between adjacent strips. In the present application of this method, it has been used for both supersonic and hypersonic external flow layers, with the lower boundary of the external flow defined by the viscous sublayer thickness.

A key parameter to be derived from the external flowfield analysis is the real part of the complex pressure perturbation parameter

$$\Pi_r = \frac{(p_w')_r}{\rho_L u_L{}^2(\varepsilon/\delta_L)} = \frac{\gamma p_e \hat{P}_{mag} \cos\phi_p}{\rho_L u_L{}^2}\left(\frac{\delta_L}{\delta}\right) \tag{9}$$

The quantity $\hat{P}_{mag}\cos\phi_p$ represents the component of the pressure perturbation in the valleys of the wavy surface. Figure 5 presents typical variations of this quantity at $M_e = 5$ where it is shown that a maximum value is attained as a function of ω and δ/λ_L. Similar results have been computed for other Mach numbers, and a correlation of the maximum pressure perturbations is shown in Fig. 6. The corresponding wave angles for maximum pressure in the valleys are presented in Fig. 7, where a comparison is made with the results of Kubota[5] at $M_e = 2.5$. The agreement is quite good at this Mach number, but not at hypersonic conditions where two-dimensional similitude normal to the waves cannot be assumed.

Combined Solution

Substituting the complex shear and pressure perturbation

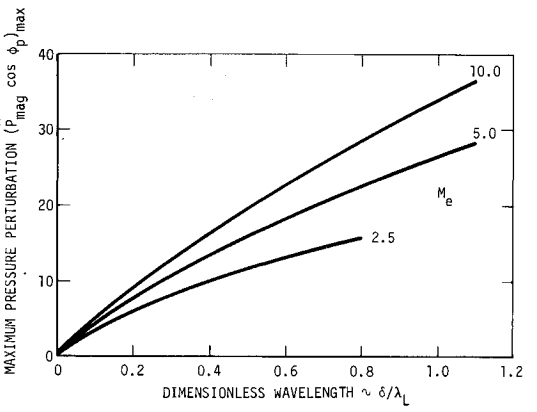

Fig. 6 Correlation of maximum pressure perturbation in surface valley; Donaldson-Conrad theory.

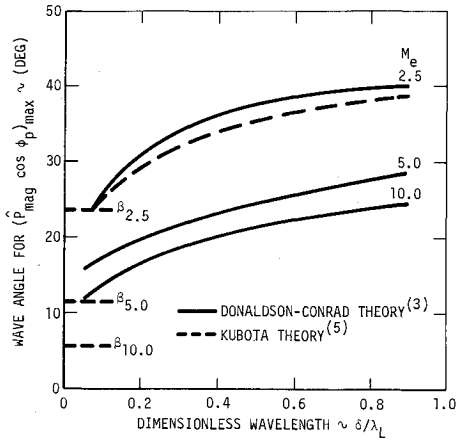

Fig. 7 Wave angles for maximum pressure perturbation in surface valley.

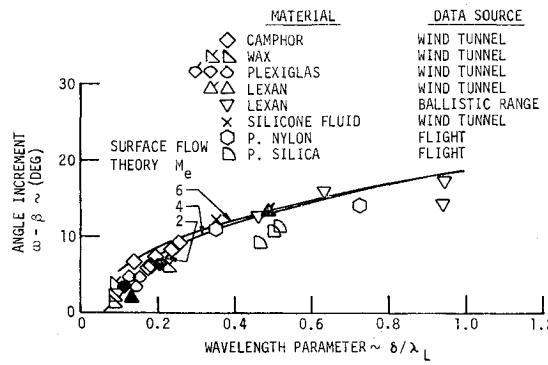

Fig. 9 Wave angle correlation for various materials.

parameters [Eqs. (7) and (9)] into the surface flow amplification rate solution [Eq. (2)] yields

$$\alpha c_i = \frac{\alpha^2 Re}{3\rho_L u_L^2}\left[\gamma p_e\left(\frac{\delta_L}{\delta}\right)\hat{P}_{mag}\cos\phi_p + \frac{2.06\gamma}{\alpha^{1/3}}\,p_e\left(\frac{\delta_L}{\delta}\right)\left(\frac{\mu_w^2}{\rho_w \tau_{w_N}}\right)^{1/2} \times \hat{P}_{mag}\sin(\phi_p + 120) - \frac{\sigma\alpha^2}{\delta_L} - g\rho_L\delta_L\right] \quad (10)$$

For the low speed, low viscosity cases considered by Craik[10] (e.g., subsonic water flow), the four terms in the bracket were all significant, and could influence the amplification or damping of disturbances. However, when the present authors[2] applied this equation to high-viscosity surface flows (e.g., teflon) under supersonic conditions, it was determined that the surface tension and body force terms were always negligible. The pressure and shear perturbation terms were always found to be dominant for these conditions. The pressure perturbation produces an amplifying effect because it has a component acting in the valleys of the disturbed surface. Physically the resulting downward force on the valley and upward force on the crest tends to increase the disturbance amplitude. The effect of the shear perturbation can be amplifying or damping, depending on the magnitude of the pressure phase angle, ϕ_p. For Craik's subsonic cases ($\phi_p = 0$), the shear perturbation is amplifying, since it tends to pile up material on the crests of the waves. However, at supersonic flow conditions, the pressure phase angle can become quite large ($\phi_p > 60°$), which according to Eq. (10) causes the shear perturbation term to be negative (a damping effect). Therefore, when $\phi_p > 60°$, the shear perturbation in supersonic flow tends to remove material from the crests and deposit it in the valleys of the disturbed surface flow. This is one of the essential differences between subsonic and supersonic shear perturbation behavior.

By neglecting the surface tension and body force terms in Eq. (10), assuming $\gamma = 1.4$, and introducing a dimensional amplification rate, $\bar{\alpha}\bar{c}_i = \alpha c_i(u_L/\delta_L)$, one obtains

$$\bar{\alpha}\bar{c}_i = 18.4\left(\frac{\delta_L}{\lambda_L}\right)^3 \frac{p_e}{\mu_L}\frac{\hat{P}_{mag}\cos\phi_p}{\delta/\lambda_L} \times \left[1 + \frac{1.1\mu_w^{2/3}\lambda_L^{1/3}}{\delta_L(\rho_w\tau_w)^{1/3}}\frac{\sin(\phi_p+120)}{\cos\phi_p}\right] \sim (\sec^{-1}) \quad (11)$$

The following section considers the application of Eq. (11) for evaluating crosshatch pattern characteristics in supersonic flow. Experimental data is used to enhance the theoretical techniques and to serve as an indicator of the accuracy of the predictions.

III. Application of Theory

Wave Angle Prediction

A significant result of Eq. (11) is that the amplification rate is directly proportional to the pressure perturbation component, $\hat{P}_{mag}\cos\phi_p$. Therefore, the maximum values of this quantity shown in Figs. 5 and 6 represent peak amplification conditions for selecting a preferred pattern geometry. For a specified Mach number (M_e) and wavelength ratio (δ/λ_L), the pattern wave angle (ω) is determined from the external flow pressure perturbation solutions as shown in Fig. 7. To partially eliminate the effects of Mach number on pattern wave angle, it is expedient to present these results as a difference between the wave angle and Mach angle ($\omega - \beta$). This format is used in Figs. 8 and 9 to present a comparison between theory and experiment[13] for the dependence of pattern wave angle on the wavelength ratio. The agreement is shown to be quite good over a large range of Mach numbers and wavelength ratios. A simple correlation of these results is

$$(\omega - \beta) = \begin{cases} 29.9(\delta/\lambda_L)^{0.8} & \text{for } \delta/\lambda_L < 0.6 \\ 17.5(\delta/\lambda_L)^{0.19} & \text{for } \delta/\lambda_L \geq 0.6 \end{cases} \quad (12)$$

Neutral Stability Prediction

For application to supersonic flow conditions, it is assumed that the pressure phase angle is approximately 75°, so that the

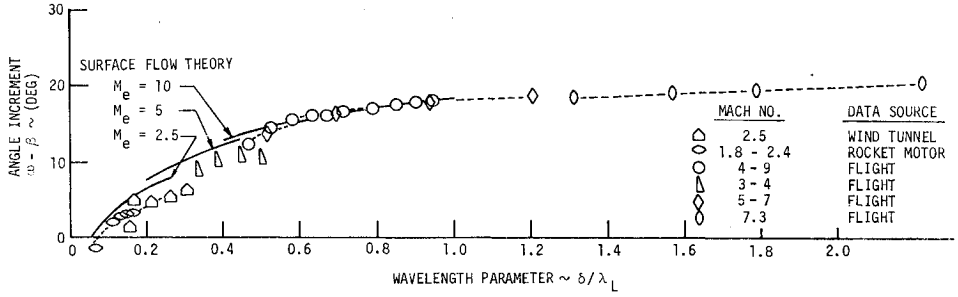

Fig. 8 Wave angle correlation for teflon.

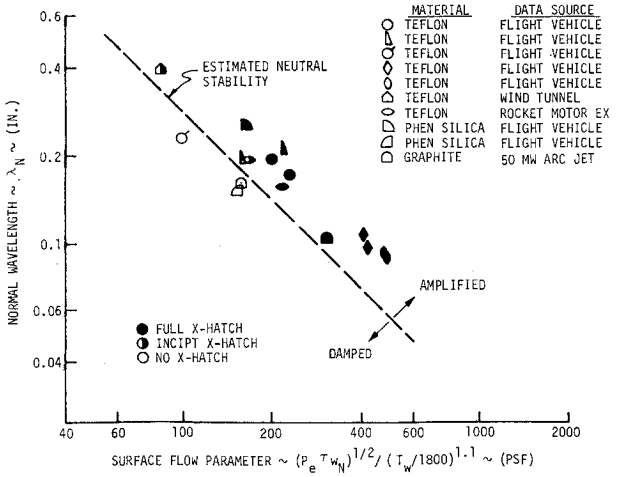

Fig. 10 Neutral stability correlation—High temperature materials.

quantity, $\sin(\phi_p+120)/\cos\phi_p$ equals -1.0. Therefore, at the neutral stability condition ($\bar{x}\bar{c}_i = 0$) corresponding to the preferred wave angle, the bracketed part of Eq. (11) yields

$$\lambda_{L_o} = 0.75\delta_L{}^3\rho_w\tau_w/\mu_w{}^2 \tag{13}$$

By utilizing a perfect gas law and a viscosity law

$$\rho_w \sim p_e\tilde{M}_w/T_w \quad \text{and} \quad \mu_w \sim \tilde{M}_w{}^{0.5}T_w{}^{0.6} \tag{14}$$

the functional dependence of the wavelength for neutral stability may be written

$$\lambda_{L_o} \sim \delta_L{}^3 p_e\tau_w/T_w{}^{2.2} \quad \text{or} \quad \lambda_{N_o} \sim \delta_L{}^3 p_e\tau_{w_N}/T_w{}^{2.2} \tag{15}$$

Attempts to correlate experimental data in terms of this expression were of limited success, primarily due to difficulties in evaluating the surface flow thickness, δ_L. Even for a relatively well-characterized material like teflon, the melt layer properties at characteristic ablation temperatures are uncertain. In order to circumvent this problem, an assumption is made that at the neutral stability condition the wavelength normal to the wave crests is proportional to the surface flow thickness (e.g., $\lambda_{N_o} \sim \delta_L$). This assumption is based on Nachtscheim's numerical results[8] and the present author's data correlations.[13] Substituting for δ_L in Eq. (15), the normal wavelength for neutral stability is

$$\lambda_{N_o} = 2.35(T_w/1800.)^{1.1}/(p_e\tau_{w_N})^{1/2} \sim \text{Ft} \tag{16}$$

for units of T_w in °R and p_e and τ_{w_N} in lb/ft^2. The proportionality constant for this relation was obtained from the correlation of experimental data presented in Fig. 10. This correlation is applicable to high-temperature materials (e.g., teflon and phenolic silica) under steady-state ablation conditions. It has been shown by the present authors[2] that it is invalid for transient ablation conditions where the surface flow thickness is time dependent. The "no-crosshatch" data points in Fig. 10 represent the wavelengths that would exist if patterns did occur; these normal wavelengths are calculated from the wave angle correlations of Figs. 8 and 9 in conjunction with the correlation of streamwise wavelengths discussed in the following paragraph. It is noted that the flight vehicle data points were evaluated at the altitude corresponding to maximum surface pressure on the body.

Wavelength Predictions

The observed pattern wavelengths are expected to correspond to theoretically derived conditions of maximum amplification. However, the surface flow amplification rate solution [Eq. (11)] is only applicable in the vicinity of the long wavelength neutral stability condition. There is presently no mechanism in the solution for predicting the wavelength where maximum amplification occurs. An alternate technique employed by the authors is to utilize the neutral stability solution [Eq. (15)] to correlate experimental wavelength data under the premise that the maximum amplification condition is not far removed from the neutral stability point. This is reasonable in light of Nachtscheim's results.[8] It is further assumed that the material is in a steady-state high-ablation mode, so that the surface flow thickness is inversely proportional to the surface shear ($\delta_L \sim 1/\tau_w$). Since $\tau_w \sim p_e{}^{0.85}$ for turbulent flow, Eq. (15) has the functional dependence, $\lambda_L \sim p_e{}^{-0.7}$ for a given material with a constant surface temperature.

A plot of experimental streamwise wavelength data as a function only of pressure is presented in Fig. 11 for several materials. For the flight vehicles, the maximum pressures are represented. It is shown that the data are correlated quite well by the functional relation, $\lambda_L \sim p_e{}^{-0.77}$, which is close to the theoretically derived result. However, it must be noted that this correlation is valid only for steady-state ablation conditions. Deviations from this simple pressure correlation for transient flow conditions have been discussed in Refs. 2 and 13. It is noted that Williams[14] also correlated wavelength data as a function only of pressure.

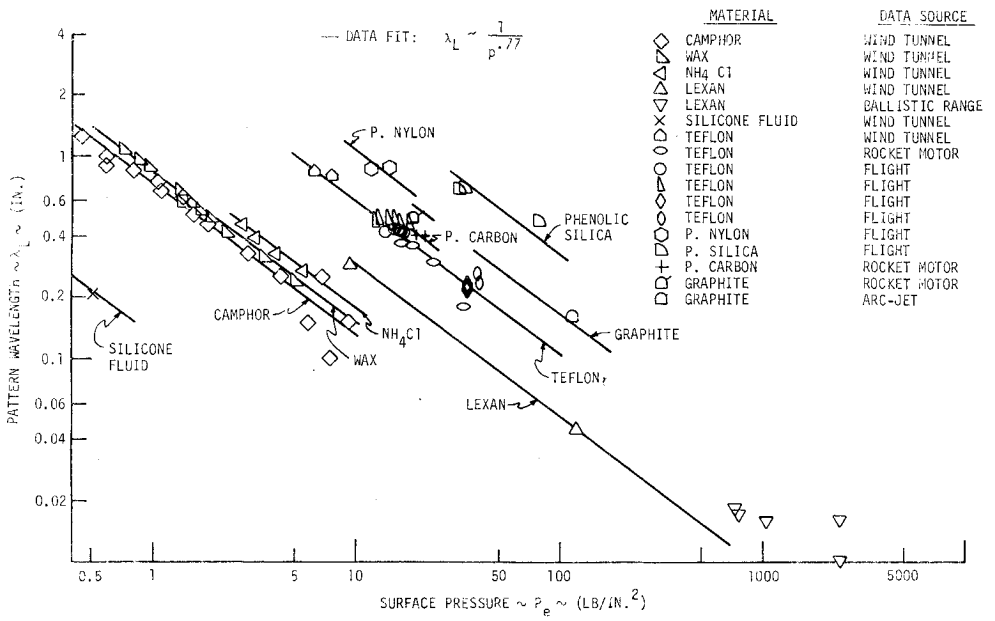

Fig. 11 Wavelength as a function of pressure for various materials.

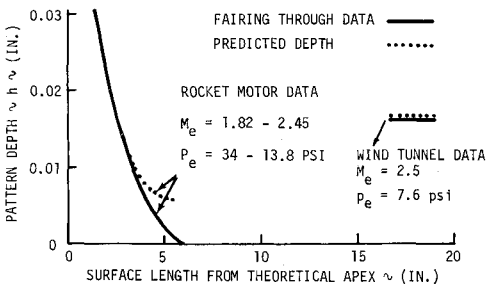

Fig. 12 Pattern depth predictions for teflon compared to ground test data.

Pattern Depth Predictions

The pattern depth history is related directly to the amplitude of the surface waves. From Eq. (1), the depth can be expressed in the functional form

$$h \sim \varepsilon \sim \varepsilon_o \exp\left\{\int_0^t \bar{\alpha}\bar{c}_i\, dt\right\} \tag{17}$$

The dimensional amplification rate $\bar{\alpha}\bar{c}_i$ is obtained from Eq. (11), with the bracketed part simplified by Eqs. (14–16). The result is

$$\bar{\alpha}\bar{c}_i = 18.4\left(\frac{\delta_L}{\lambda_L}\right)^3 \frac{p_e}{\mu_L} \frac{\hat{P}_{\text{mag}} \cos\phi_p}{\delta/\lambda_L} \cdot \left[1. - \frac{1.77(T_w/1800)^{0.73}}{(p_e \tau_{w_N})^{1/3} \lambda_N^{\,2/3}}\right] \tag{18}$$

If one assumes that the viscosity (μ_L) and depth ratio (δ_L/λ_L) are invariant for a given material, then these parameters can be combined into a single constant. For the case of high-temperature ablating materials, this constant has been determined from correlations of experimental pattern depth data using Eqs. (17) and (18). The resulting expression for pattern depth is

$$h = 3.8 \times 10^{-4} \exp\left\{\int_0^t K_m p_e \frac{\hat{P}_{\text{mag}} \cos\phi_p}{\delta/\lambda_L} \cdot \left[1. - \frac{1.77(T_w/1800)^{0.73}}{(p_e \tau_{w_N})^{1/3} \lambda_N^{\,2/3}}\right] dt\right\} \tag{19}$$

where $K_m = 1.9 \times 10^{-5}$ for teflon and 9.4×10^{-6} for phenolic silica in units of ft²/(lb-sec) for p_e in lb/ft² and h in ft.

It may be noted that the pattern depth is an exponential function of the surface pressure, which partially explains the pattern variation previously noted in Fig. 1. Pattern depth predictions using Eq. (18) have been performed for teflon bodies in ground and flight test environments. Figure 12 presents a comparison between measured and predicted pattern depths for wind tunnel and rocket motor test conditions. The measured results actually represent a mean fairing through relatively wide data bands. The agreement is shown to be quite good for both cases. In these tests, the flow conditions and surface temperatures were nearly constant with time so that the amplification rate $\bar{\alpha}\bar{c}_i$ could also be assumed constant; therefore, the integral term in Eq. (18) was directly proportional to the model exposure time. This is not the situation with re-entry flight vehicles, where the flow conditions vary with time. For these cases, the amplification rate was computed at various times along the trajectory and numerically integrated to determine the pattern depth history. A comparison between the predicted depths and the depths measured on five recovered teflon flight vehicles is presented in Fig. 13. The agreement is not as good as obtained with ground experiments, but the general trends are reasonably well predicted by this method of analysis. It is significant that vehicle *E*, which did not have any observable crosshatch patterns, was also not predicted to have patterns (e.g., this data point fell in the damped region to the left of the neutral stability boundary of Fig. 10).

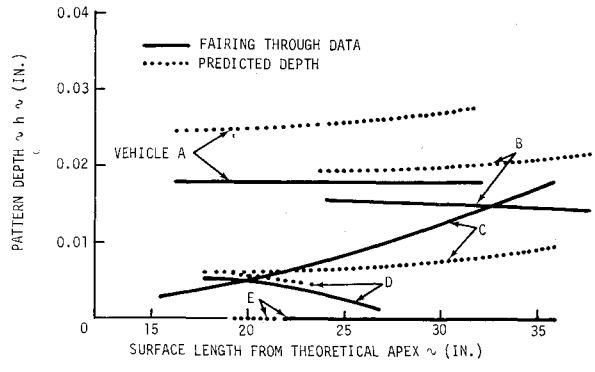

Fig. 13 Pattern depth predictions for teflon compared to flight test data.

The details of predicting pattern onset, depth, wavelength, and wave angle by this surface flow approach is demonstrated in the Appendix by way of a numerical example. The calculations are performed for one location on the teflon rocket motor model shown in Fig. 1.

IV. Conclusions

It has been shown that the three-layer model surface flow approach correlates much of the experimental cross-hatching data and can effectively predict pattern characteristics. Some of the significant results obtained with this approach are as follows: 1) At supersonic flow conditions, the dominant amplifying and damping terms in the surface flow stability equation are the pressure and shear perturbations, respectively. The surface tension and body force terms are negligible. 2) The external flow pressure perturbation field determines the variation of pattern wave angle with wavelength, independent of surface flow properties. 3) The amplification rate solution predicts a strong influence of surface flow thickness on the conditions for neutral stability. For conditions where the wavelength is proportional to surface flow thickness, a neutral stability boundary has been defined. 4) The neutral stability correlation shows that instability is promoted by increasing pressure and shear, and decreasing surface temperature. 5) Pattern wavelengths are predicted to be a function only of surface pressure for a given material at steady-state ablation conditions. For transient flow conditions, the wavelength is also a strong function of the surface flow thickness. 6) Pattern depth is an exponential function of the time-integrated amplification rate. For a given material, the surface pressure is the dominant parameter.

There are several areas where the surface flow approach can be improved. In particular, the relationship between wavelength and surface flow thickness needs to be established, rather than the assumption of a direct proportionality between the two parameters. The approach should also be investigated at low Mach number conditions where the relative effects of surface tension, body forces, and phase lags may be significantly different than at supersonic flow conditions. In particular, the magnitude and phase of the shear perturbation parameter needs to be better characterized, including experimental confirmation.

Appendix: Numerical Example of Crosshatch Pattern Predictions

Given

A teflon cone of 4.5° half-angle (Fig. 1) exposed to a rocket exhaust flow for 5.65 sec. Method of characteristics solutions for the inviscid flowfield coupled to turbulent boundary-layer solutions and heat-shield ablation analyses provided the following information at $x = 2.7$ in. from tip (8.6 in. from base of model); $p_e = 2830$ lb/ft², $M_e = 2.45$, $\delta = 0.045$ in., $\tau_w = 33.2$ lb/ft², $T_w = 1800°R$ (steady-state ablation).

Computations

1) Determine wavelength that would exist if patterns occurred. From Fig. 11, $\lambda_L = 0.35$ in.

2) Determine corresponding wave angle

$$\delta/\lambda_L = 0.045/0.35 = 0.13$$

$$\beta = \sin^{-1}(1/M_e) = \sin^{-1}(1/2.45) = 24°$$

From Fig. 9, $\omega - \beta = 3.5°$, . . $\omega = 27.5°$.

3) Determine if conditions lead to pattern amplification

$$\lambda_N = \lambda_L \sin\omega = 0.35 \sin(27.5) = 0.161 \text{ in.}$$

$$p_e \tau_{w_N} = 2830(33.2)\sin(27.5) = 4.34 \times 10^4 \text{ lb}^2/\text{ft}^4$$

$$(p_e \tau_{w_N})^{1/2}/(T_w/1800)^{1.1} = 208 \text{ lb/ft}^2$$

The neutral stability plot of Fig. 10 shows this to be an unstable condition so that the patterns will amplify. Therefore, the tentative values of λ_L and ω are now the predicted values.

4) Determine amplification rate. From Fig. 6

$$\hat{P}_{\text{mag}} \cos\phi_p/(\delta/\lambda_L) = 3.5/0.13 = 26.9$$

$$\bar{\alpha}\bar{c}_i = K_m p_e \frac{\hat{P}_{\text{mag}}}{\delta/\lambda_L} \cos\phi_p \left[1 - \frac{1.77(T_w/1800)^{0.73}}{(p_e \tau_{w_N})^{1/3}(\lambda_N)^{2/3}}\right]$$

$$= 1.9 \times 10^{-5}\,(2830)(26.9)\left[1 - \frac{1.77(1)}{(4.34 \times 10^4)^{1/3}(0.0134)^{2/3}}\right]$$

$$= 0.145\,(\text{sec}^{-1})$$

5) Determine pattern depth for the case of constant flow conditions and surface temperature

$$\int_0^t \bar{\alpha}\bar{c}_i\,dt = \bar{\alpha}\bar{c}_i\, t = 0.145(5.65) = 0.82$$

$$h = 3.8 \times 10^{-4} \exp\left[\int_0^t \bar{\alpha}\bar{c}_i\,dt\right]$$

$$= 3.8 \times 10^{-4}(2.27) = 8.62 \times 10^{-4} \text{ ft}$$

$$= 0.0103 \text{in.}$$

Table 1 gives a comparison between the preceeding predictions and the experimental data.

Table 1 Comparison between predictions and experimental data

Pattern Characteristic	Experimental	Predicted
wavelength, λ_L	0.27–0.40 in.	0.35 in.
wave angle, ω	26–28.5°	27.5°
pattern depth, h	0.006–0.019 in.	0.0103 in.

References

[1] White, C. O., Grabow, R. M., and Moody, H. L., "Final Report, Small Vehicle Dynamics Study II, Crosshatch Studies: Volume I—Data Survey and Data Processing," RSO Publication U-4972, Oct. 1971, Philco-Ford, Newport Beach, Calif.

[2] White, C. O. and Grabow, R. M., "Final Report, Small Vehicle Dynamics Study II, Crosshatch Studies, Volume II—Theory, Correlations, and Criteria," RSO Publication U-4972, Nov. 1971, Philco-Ford, Newport Beach, Calif.

[3] Conrad, P., Donaldson, C. duP., and Snedeker, R., "A Study of the Modal Response Approach to Patterned Ablation Including Experiment Definition," SAMSO TN-70-213, April 1970, U.S. Air Force, El Segundo, Calif.

[4] Inger, G. R., "Compressible Boundary Layer Flow Past a Swept Wavy Wall with Heat Transfer and Ablation," VKI Tech. Note 67, Dec. 1970, von Kármán Institute; also in *Astronautica Acta*, Vol. 16, Pergamon Press, 1971.

[5] Lees, L. and Kubota, T., "Research on Fluid Mechanics of Striating Ablation," GALCIT Progress Rept. 1–3, 1969, California Inst. of Technology, Pasadena, Calif.

[6] Gold, H., Probstein, R. F., and Scullen, R., "Inelastic Deformation and Crosshatching," *AIAA Journal*, Vol. 9, No. 10, Oct. 1971, pp. 1904–1910.

[7] Lane, F., "Viscoelastic-Material Version of the Self-Excitation Analysis for Striations of Ablating or Deforming Materials in Supersonic Flows with Turbulent Boundary Layers," KLD Tech. Rept. 1, July 1971, KLD Associates, New York.

[8] Nachtsheim, P. R., "Stability of Crosshatched Wave Patterns in Thin Liquid Films Adjacent to Supersonic Streams," *The Physics of Fluids*, Vol. 13, No. 10, Oct. 1970, pp. 2432–2447.

[9] Hains, F., "Crosshatched Erosion Patterns at the Beach," *The Physics of Fluids*, Vol. 14, No. 12, Dec. 1971.

[10] Craik, A. D., "Wind Generated Waves in Thin Liquid Films," *Journal of Fluid Mechanics*, Vol. 26, Pt. 2, 1966, pp. 369–392.

[11] Nayfeh, A. and Saric, W., "Body Force Effects on the Stability of a Liquid Layer Film," Rept. SC-RR-70-722, Nov. 1970, Sandia Lab., Albuquerque, N. Mex.

[12] Segal, A., "An Experimental Investigation of the Turbulent Boundary Layer Over a Wavy Wall," PhD. thesis, April 1971, California Institute of Technology, Pasadena, Calif.

[13] White, C. O. and Grabow, R. M., "Surface Patterns—Comparison of Experiment with Theory," AIAA Paper 72-313, San Antonio, Texas, 1972.

[14] Williams, E., "Experimental Studies of Ablation Surface Patterns and Resulting Roll Torques," *AIAA Journal*, Vol. 9, No. 7, July 1971, pp. 1315–1321.